Exact analysis of ultrahigh laser-induced acceleration of electrons by cyclotron autoresonance

Yousef I. Salamin*
Theoretische Quantendynamik, Fakultät für Physik, Universität Freiburg, Hermann-Herder-Strasse,3, D-79104 Freiburg, Germany

F. H. M. Faisal†
Fakultät für Physik, Universität Bielefeld, 33615 Bielefeld, Germany

Christoph H. Keitel‡
Theoretische Quantendynamik, Fakultät für Physik, Universität Freiburg, Hermann-Herder-Strasse, 3, D-79104 Freiburg, Germany
(Received 11 November 1999; published 19 October 2000)

We study the relativistic dynamics of a single electron in a plane-wave laser field and a static magnetic field oriented along the laser propagation direction. A set of exact solutions, that demonstrate acceleration to TeV energies in vacuum by the mechanism of resonance between the electron cyclotron frequency and the Doppler-shifted laser frequency, is presented. Forward velocity focusing is demonstrated, the radiation losses are shown to be negligible, and the frequency distribution of the weak radiation scattered by the electron undergoing the acceleration is discussed.

PACS number(s): 42.65.−k, 52.40.Nk, 42.50.Vk, 52.75.Di

I. INTRODUCTION

There has been a renewed interest lately in the problem of particle acceleration to very high energies utilizing lasers and various other types of electromagnetic fields [1–15]. A considerable amount of work on the subject was published earlier [16–23]. This interest is driven by the need to develop alternatives to the costly and huge conventional particle accelerators, and is motivated by the advent of state-of-the-art ultrahigh intensity laser systems capable of delivering short-duration pulses of a small number of field cycles or even subcycles [24,25].

Over a decade ago a scheme for accelerating electrons using a laser field and a uniform axial magnetic field was suggested [21–23]. The mechanism of acceleration is based on self-sustained cyclotron resonance [26,27] and the scheme employing it came to be known as the autoresonance laser accelerator (ALA) scheme. The idea of an ALA was originally developed within the context of a study of the dynamics of a cold electron beam in the presence of a plane-wave laser field propagating along an axial magnetic field. In an interesting discussion of the relativistic dynamics of charges in electromagnetic fields via an eigenspinor approach [13], it was recently noted that analytical solutions which led to proposals of the ALA scheme have been *indirect* [21–23,26,27].

The purpose of the present paper is to derive exact working equations for the ALA scheme by a direct solution to the relevant single-particle equations of motion. Trajectory equations, energy expressions, and velocity components will all be derived under the autoresonance condition expressed in Eq. (1) below. Our analysis is restricted to the single-particle case, with the understanding that it may easily be adapted to handle an assembly of electrons, which better represents the practical situation, by averaging over an appropriate distribution of initial velocities. We carry out the derivations directly in the laboratory frame of reference. Our approach leads to a set of simple equations for the electron dynamics employing the phase of the laser field as a convenient parameter. The equations are easily interpreted, and used to predict the outcome of laser accelerator experiments made possible by present-day and future advances in laser technology. For example, on the basis of our equations using only simple arithmetic one can calculate that an electron will be accelerated to 1.5 TeV as a result of interaction with 1.5 field cycles of a laser beam of intensity around 10^{22} W/cm^2, and in the presence of a magnetic field of strength 1000 T over only 15 m. The equations are also used for such ends as calculation of the associated radiation losses and analysis of the spectra of the emitted radiation. The importance of an analytic solution lies in the fact that it leads to deeper insight into the problem at hand, and hence to a better understanding of the physics involved. For example, on the basis of our equations we can easily demonstrate focusing of the electron momentum, and hence its velocity in the forward direction.

When a fast electron is injected at the speed v_0 along the propagation direction of a (plane-wave) laser field of frequency ω_l and in the added presence of a uniform magnetic field of strength B_s, also aligned along the same direction, it follows a wiggly helical path [28] and may pick up energy and be accelerated. The energy gain can be arbitrarily large, provided the electron motion initially satisfies *the resonance condition*

$$r \equiv \frac{\omega_c}{\omega_l}\sqrt{\frac{1+\beta_0}{1-\beta_0}} = 1. \tag{1}$$

In Eq. (1), $\beta_0 = v_0/c$, i.e., the initial electron speed normalized by the speed of light c, $\omega_c = eB_s/(mc)$ is the cyclotron

*On leave from Physics Department, Birzeit University, P.O. Box 14, Birzeit, West Bank, via Israel. Electronic address: ysalamin@science.birzeit.edu
†Electronic address: ffaisal@physik.uni-bielefeld.de
‡Electronic address: keitel@physik.uni-freiburg.de

frequency of the electron motion in the uniform magnetic field, and $-e$ and m are the charge and mass, respectively, of the electron. Denote the electric and magnetic components of the laser field by $\boldsymbol{E}_l$ and $\boldsymbol{B}_l$, respectively, and the electron velocity vector by $\boldsymbol{v}$. For ultrarelativistic electrons, the strength of the magnetic component $-(e/c)\boldsymbol{v}\times\boldsymbol{B}_l$ of the force is comparable to that of the electric component $-e\boldsymbol{E}_l$. So, as soon as the front edge of the laser pulse (say a plane wave with sharp turn-on and turn-off) catches up with the fast forward-moving electron, the electric component of the laser field will accelerate it in a direction opposite to that of polarization. As a result, the electron velocity vector acquires a transverse component. This, in turn, leads to a violent change in the direction of motion of the electron brought about by the $-(e/c)\boldsymbol{v}\times\boldsymbol{B}$ force, where now $\boldsymbol{B}=\boldsymbol{B}_l+\boldsymbol{B}_s$. The overall effect, when the above-mentioned resonance condition is met, will be to launch the electron along a helical path with a slowly increasing transverse radius and a fast-widening pitch. The axis of the semihelical trajectory will be parallel to the lines of $\boldsymbol{B}_s$. In other words, the transverse component of the position vector of the electron will *gyrate* around the forward direction at the rate $\omega_c/2\pi$. At the same time, the electron will be advancing forward at a speed v_z.

Recall that the electron energy-gain (or -loss) rate, due to interaction with the electromagnetic field configuration described above, is governed by the equation

$$\frac{d\mathcal{E}}{dt}=-e\boldsymbol{v}\cdot\mathbf{E}_l. \tag{2}$$

Thus if conditions could be found that will result in $\boldsymbol{v}$ and $\mathbf{E}_l$ maintaining the same orientation relative to one another (more accurately, an angle between their directions in the range $\pi/2$ to $3\pi/2$), then continued absorption of energy by the electron from the radiation field will be guaranteed. For this to happen, two conditions must be met. (a) v_z should quickly approach the phase velocity of the laser pulse, this being $v_{ph}=c$ for a plane wave. With $v_z\approx v_{ph}$ the electron will move in phase with the accelerating component of the laser field $\boldsymbol{E}_l$; otherwise it will quickly slip behind the pulse and be decelerated. (b) The cyclotron frequency of the electron around the windings of the helical trajectory should, at least approximately, match the rate at which it *sees* the vector $\boldsymbol{E}_l$ go around the propagation direction of the laser. (This is in the case of a circularly polarized wave; a linearly polarized wave may be thought of as the superposition of left- and right-handed circularly polarized waves of $1/\sqrt{2}$ times the amplitude.)

With a strong $-(e/c)\boldsymbol{v}\times\boldsymbol{B}_l$ force, made possible by shining an ultra-high-intensity laser beam on an already relativistic electron, condition (a) may be approximately met. On the other hand, if the values of β_0, ω_l, and B_s satisfy Eq. (1) initially, then condition (b) will be met as well. Equation (1) is equivalent to $\omega_c=\tilde{\omega}_0$, where $\tilde{\omega}_0$ is the Doppler-shifted laser frequency as seen by the electron initially. This is another way of expressing condition (b).

We understand that a laser pulse may best be modeled by a Gaussian-Hermite beam, and that a plane-wave description is only approximate [3,10,29]. Nevertheless, the idealized plane-wave description has the advantage of being amenable to analytic manipulations which lead to solutions to the equations of motion of the electron in closed analytic form. Conversely, the more complicated Gaussian-Hermite description can only be employed *exactly* in numerical simulations, or else may be used in conjunction with many (well-justified) approximations [3,9] involving the various beam and optical-element design parameters. In addition, plane-wave results may be very helpful in benchmarking the codes to be used in handling more realistic situations numerically.

We have recently gone beyond the plane-wave analysis [14] by working out equations for the ALA scheme employing a description for the short ultraintense laser pulse in terms of a $\sin^2$ envelope, a middle ground between the plane-wave and Gaussian-Hermite descriptions. Still, the resulting working solutions turned out to be quite complex.

The laser-induced electron acceleration and the accompanying radiation of harmonics achieved here compares to what one encounters in, for example, laser-assisted scattering at an ionic core or laser-assisted ionization, where the static field is replaced by the Coulomb field. These processes were discussed intensively in the literature [30].

The general electron trajectory solutions in the electromagnetic field configuration described above will be reviewed, and their autoresonance forms will be discussed, in Sec. II. Following the same pattern of exposition, a discussion of the energy equations will be presented in Sec. III. This will be followed by a calculation of the radiation losses where estimates will show that those are negligibly small under autoresonance. Section V will be devoted to a spectral analysis of the weak radiation emitted by the accelerated electron. Frequency spectra for emission along the initial (forward) direction of motion of the electron, and slightly away from this direction, will be the subject of investigation in this section. We summarize our results and make some concluding remarks in Sec. VI.

II. ELECTRON TRAJECTORY EQUATIONS

A. Preliminary considerations

Working classically and fully relativistically, we recently obtained the trajectory equations of a single electron in the simultaneous presence of a uniform magnetic field and an elliptically polarized plane-wave laser field [14]. In a more recent paper [31] the forward and backscattered radiation spectra associated with this system were investigated analytically as well. We devote this subsection to a review of the basic equations in order to make this paper as self-contained as possible.

Our system consists of a single electron, charge $-e$ and mass m, subjected to a monochromatic plane-wave laser field of amplitude A_l propagating in the positive z direction. In addition, a uniform magnetic field of strength B_s pointing also along $+z$ is present. A schematic of the geometry of the system is shown in Fig. 1.

The laser plus magnetic fields may be modeled by the vector potential

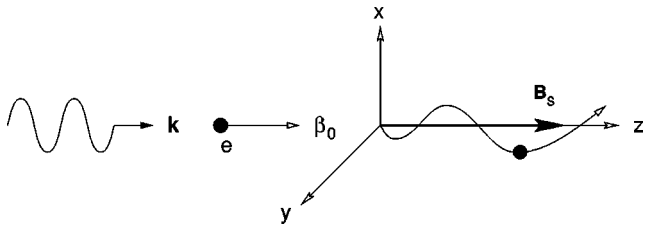

FIG. 1. Schematic of the electron interaction with and dc magnetic fields.

$$\mathbf{A}=A_l[\hat{\mathbf{i}}\delta\cos\eta+\hat{\mathbf{j}}\sqrt{1-\delta^2}\sin\eta]-\frac{B_s}{2}(\hat{\mathbf{i}}y-\hat{\mathbf{j}}x). \tag{3}$$

In Eq. (3), $\eta=\omega_l t-\mathbf{k}\cdot\mathbf{r}$, where ω_l and $\mathbf{k}$ are the laser frequency and propagation vector, respectively, and t and $\mathbf{r}$ are the time and space coordinates of the electron. Furthermore, $\hat{\mathbf{i}},\hat{\mathbf{j}}$, and $\hat{\mathbf{k}}$ are unit vectors in the directions of positive x, y, and z, respectively. As noted above, we will take $\mathbf{k}=k\hat{\mathbf{k}}=(\omega_l/c)\hat{\mathbf{k}}$, c being the speed of light in vacuum. The radiation part in Eq. (3) describes an elliptically polarized plane wave, with δ giving the degree of ellipticity. From $\mathbf{A}$ one derives the electric and magnetic fields, as usual, using

$$\mathbf{E}=-\frac{1}{c}\frac{\partial\mathbf{A}}{\partial t},\quad \boldsymbol{B}=\boldsymbol{\nabla}\times\mathbf{A}. \tag{4}$$

Motion of the electron in these fields is governed by the following equations for the electron momentum $\mathbf{p}=\gamma mc\boldsymbol{\beta}$ and its energy $\mathcal{E}=\gamma mc^2$:

$$\frac{d\mathbf{p}}{dt}=-e(\mathbf{E}+\boldsymbol{\beta}\times\mathbf{B}),\quad \frac{d\mathcal{E}}{dt}=-ec\boldsymbol{\beta}\cdot\mathbf{E}. \tag{5}$$

Here $\gamma=(1-\beta^2)^{-1/2}$ is the Lorentz factor, and $\boldsymbol{\beta}$ is the electron velocity normalized by c. In component form, Eqs. (5) are equivalent to the following set:

$$\frac{d(\gamma\beta_x)}{dt}=-q\delta\omega_l(1-\beta_z)\sin\eta-\omega_c\beta_y, \tag{6}$$

$$\frac{d(\gamma\beta_y)}{dt}=q\sqrt{1-\delta^2}\omega_l(1-\beta_z)\cos\eta+\omega_c\beta_x, \tag{7}$$

$$\frac{d(\gamma\beta_z)}{dt}=q\omega_l[\sqrt{1-\delta^2}\beta_y\cos\eta-\delta\beta_x\sin\eta], \tag{8}$$

$$\frac{d\gamma}{dt}=q\omega_l[\sqrt{1-\delta^2}\beta_y\cos\eta-\delta\beta_x\sin\eta]. \tag{9}$$

In Eqs. (6)–(9), $\omega_c=eB_s/mc$ is the cyclotron frequency of the electron motion in the magnetic field B_s, and $q=eA_l/mc^2$ is the dimensionless intensity parameter of the laser field ($q=1$ corresponds to a laser intensity of $I\approx10^{18}$ W/cm^2). Furthermore, the scaled velocity vector has been written in component form as $\boldsymbol{\beta}=(\beta_x,\beta_y,\beta_z)$.

Subject to a general set of conditions on the initial motion of the electron (coordinates x_0,y_0, and z_0, and hence the phase η_0), and its initial scaled velocity components (β_{x0}, β_{y0}, and β_{z0}) in the given laser and magnetic-field environment, Eqs. (6)–(9) were recently solved exactly analytically [14]. Only the highlights of relevance to the present work will be recalled here. For example, the right-hand sides of Eqs. (8) and (9) are identical, so if we equate the left-hand sides and carry out the single integration, we arrive at the following useful relation:

$$\gamma(1-\beta_z)=\gamma_0(1-\beta_{z0}). \tag{10}$$

Note that, throughout this paper, the 0 subscript signifies an initial value at $t=0$ for the subscripted quantity. Another useful relation is obtained from differentiating the phase η once with respect to time:

$$\frac{d\eta}{dt}=\omega_l(1-\beta_z). \tag{11}$$

A third relation, which will play a central role in the calculation of the electron trajectories below, may be obtained by considering the derivative of a typical Cartesian coordinate with respect to the phase η, aided by Eqs. (10) and (11). With Q standing for x,y, or z, we have

$$\frac{dQ}{d\eta}=\frac{dQ}{dt}\frac{dt}{d\eta}=\frac{c}{\omega_l}\frac{\gamma\beta_Q}{\gamma_0(1-\beta_{z0})}. \tag{12}$$

Using Eq. (11) in the first term on the right-hand side of Eq. (6), and writing $\beta_y=(1/c)(dy/dt)$ in the second, yields a simple differential equation. A single integration then gives,

$$\gamma\beta_x=\gamma_0\beta_{x0}+q\delta(\cos\eta-\cos\eta_0)-\frac{\omega_c}{c}(y-y_0). \tag{13}$$

Similarly,

$$\gamma\beta_y=\gamma_0\beta_{y0}+q\sqrt{1-\delta^2}(\sin\eta-\sin\eta_0)+\frac{\omega_c}{c}(x-x_0). \tag{14}$$

Using Eqs. (13) and (14) in Eq. (12) results in the following coupled differential equations for x and y, respectively:

$$\frac{dx}{d\eta}=\frac{c}{\omega_l\gamma_0(1-\beta_{z0})}\left[q\delta(\cos\eta-\cos\eta_0)-\frac{\omega_c}{c}(y-y_0)+\gamma_0\beta_{x0}\right], \tag{15}$$

$$\frac{dy}{d\eta}=\frac{c}{\omega_l\gamma_0(1-\beta_{z0})}\left[q\sqrt{1-\delta^2}(\sin\eta-\sin\eta_0)+\frac{\omega_c}{c}(x-x_0)+\gamma_0\beta_{y0}\right]. \tag{16}$$

Equations (15) and (16) may be decoupled and solved along lines described elsewhere [15]. In particular, the following parametric equations (employing η as a convenient parameter) were obtained for the x and y positions of the electron:

$$x(\eta)=\frac{qc}{\omega_l\gamma_0(1-\beta_{z0})}\left[\frac{\delta+r\sqrt{1-\delta^2}}{1-r^2}\right]\sin\eta+\frac{c}{\omega_l\gamma_0(1-\beta_{z0})}\times\left[\frac{-\gamma_0\beta_{y0}+\frac{\omega_c}{c}x_0+q\sqrt{1-\delta^2}\sin\eta_0}{r}\right]+a\cos(r\eta)-b\sin(r\eta), \tag{17}$$

$$y(\eta)=-\frac{qc}{\omega_l\gamma_0(1-\beta_{z0})}\left[\frac{r\delta+\sqrt{1-\delta^2}}{1-r^2}\right]\cos\eta+\frac{c}{\omega_l\gamma_0(1-\beta_{z0})}\left[\frac{\gamma_0\beta_{x0}+\frac{\omega_c}{c}y_0-q\delta\cos\eta_0}{r}\right]+a\sin(r\eta)+b\cos(r\eta). \tag{18}$$

In Eqs. (17) and (18), a and b are constants to be determined from the initial conditions. Furthermore, η_0 is the phase of the laser field at $t=0$. At the risk of potentially confusing it with the magnitude of the position vector of the electron (which we do not use in this paper, in any case), we have employed r to stand for the combination

$$r=\frac{\omega_c/\omega_l}{\gamma_0(1-\beta_{z0})}. \tag{19}$$

For a reasonable set of initial conditions, we adopt the following. We assume that the front edge of the laser pulse, itself a plane wave with sharp turn-on and turn-off, catches up with the electron at the origin of coordinates at $t=0$. At this space-time point we assume further that the electron is moving with the scaled speed $\beta_0=v_0/c$ along the $+z$ axis. Under these conditions $\eta_0=x_0=y_0=0$ and $\beta_{x0}=\beta_{y0}=0$. Moreover, Eq. (19) becomes

$$r=\frac{\omega_c}{\omega_l}\sqrt{\frac{1+\beta_0}{1-\beta_0}}. \tag{20}$$

Inserting these values into Eqs. (17) and (18) yields a convenient set of parametric representations for the electron's x and y positions in terms of the radiation field phase η. An expression for $z(\eta)$ also follows along lines described elsewhere [14]. In the following subsections, we will discuss the trajectories that result from two situations differing in the laser field polarization. Before moving on to that, a remark is in order regarding the use of η in our equations. The expression $\eta=\omega_l t-(\omega_l/c)z(\eta)$ is highly transcendental. Exact expressions for z and other relevant quantities as explicit functions of the time t are hard to find in general. To the best of our knowledge, only approximate expressions which apply to certain restricted situations could be found in the past [26,27]. Thus a parametric representation of the trajectories in terms of η offers a viable alternative. All of the equations we derive below, and express in terms of η (and use in our calculations), are exact. No approximations, beyond the fact that the whole discussion is plane wave based, are involved.

B. Linear polarization

In the case of a linearly polarized plane-wave laser field, the ellipticity parameter $\delta=1$, and the vector potential takes the form

$$\mathbf{A}(\eta)=\hat{\mathbf{i}}A_l\cos\eta-\frac{B_s}{2}(\hat{\mathbf{i}}y-\hat{\mathbf{j}}x). \tag{21}$$

With the directions of laser propagation, magnetic field, and initial electron motion taken all along $+z$, the trajectory equations (17) and (18) (see also Ref. [14]) reduce to the following:

$$x_{lin}(\eta)=\frac{qc}{\omega_l}\gamma_0(1+\beta_0)\left[\frac{r\sin\eta-\sin(r\eta)}{r(1-r^2)}\right], \tag{22}$$

$$y_{lin}(\eta)=\frac{qc}{\omega_l}\gamma_0(1+\beta_0)\left[\frac{-r^2\cos\eta+\cos(r\eta)+r^2-1}{r(1-r^2)}\right], \tag{23}$$

$$z_{lin}(\eta)=\frac{c}{\omega_l}\left(\frac{1+\beta_0}{1-\beta_0}\right)\left\{\left[\frac{\beta_0}{1+\beta_0}+\frac{q^2}{4}\frac{3+r^2}{(1-r^2)^2}\right]\eta+\frac{q^2}{8}\frac{\sin(2\eta)}{(1-r^2)}-\frac{q^2}{2}\left[\frac{(1+r)^2\sin[(1-r)\eta]+(1-r)^2\sin[(1+r)\eta]}{(1-r^2)^3}\right]\right\}. \tag{24}$$

Equations (22)–(24) parametrize the electron trajectory in terms of η. In other words, as a result of interaction with N field cycles, these equations yield a three-dimensional (3D) trajectory for the electron when η is allowed to evolve from $\eta_0=0$ (corresponding to injection at $t=0$) to $\eta=2\pi N$ [which corresponds to extraction at $t=\eta/\omega_l+z(\eta)/c$, or better after the electron is left behind an N field-cycle pulse, where N may be an integer or a fraction thereof.] A typical 3D electron trajectory calculated over interaction with $N=100$ field cycles (η values range from 0 to 200π) on the basis of Eqs. (22)–(24) is given in Fig. 2(a). For the set of parameters describing the laser field, the magnetic field, and the initial electron motion employed to produce this figure, $r=0.044612$, i.e., the system does not meet the resonance condition alluded to in the Secs. I and II A. The electron in this case follows a wiggly helical path whose axis is parallel

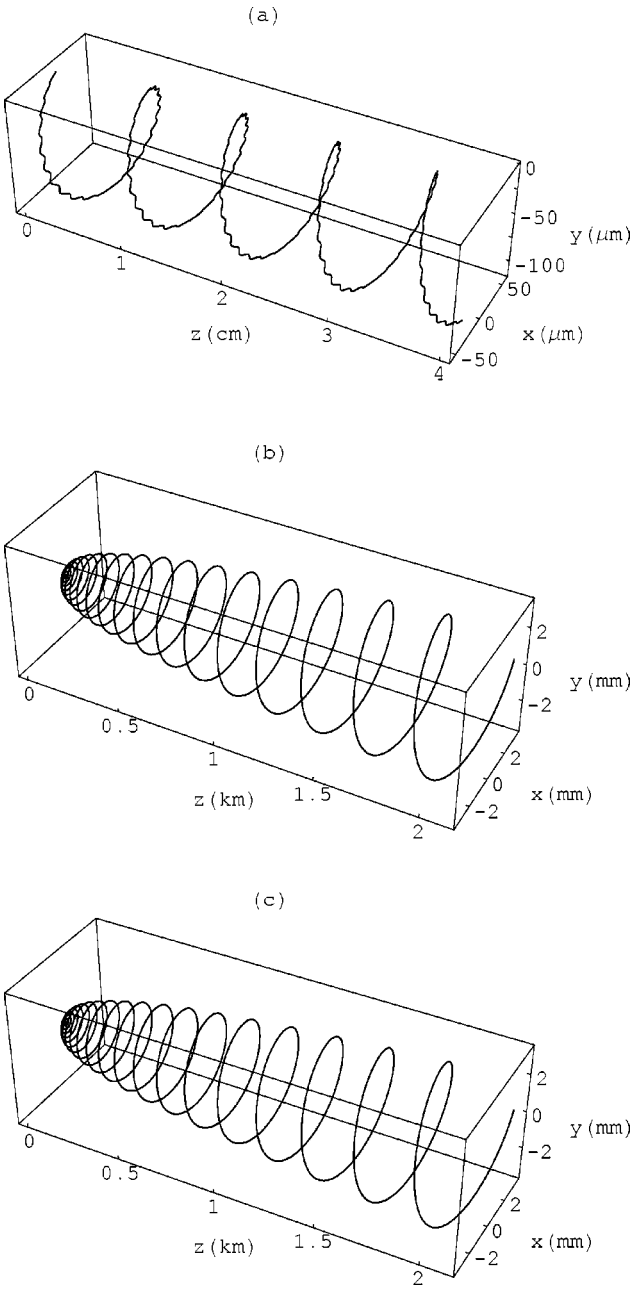

FIG. 2. Electron trajectories in a linearly polarized plane-wave laser field and a uniform magnetic field. Data used to produce these trajectories were generated from parametric representations [Eqs. (22)–(27)], by allowing η to evolve from an initial value of zero to a final value of 200π. This corresponds to an interaction of the electron with 100 field cycles. The other parameters are wavelength $\lambda = 800$ nm, intensity $I \approx 10^{18}$ W/cm^2 (or q=1), and $B_s = 30$ T. (a) Off-resonance, with $\gamma_0 = 10$ ($E_0 \approx 4.5$ MeV) and hence $r \approx 0.044612$. (b) Near-resonance, with $r = 1.001$. (c) Exact resonance, with $r = 1$.

to the common direction of $\mathbf{B}_s$ and $\mathbf{k}$. The wiggles are due to the fact that $\boldsymbol{B}_l$ is oscillatory, and hence is the force it exerts on the electron.

Of more interest to us, in the present paper, are the cases of *near resonance* ($r \approx 1$) and *exact resonance* ($r = 1$). For values of the initial electron energy, the magnetic-field strength, and the laser frequency that make $r = 1.001$, for example, the trajectory departs markedly from its *off-resonance* counterpart. Instead of following the wiggly helical path of Fig. 2(a), the electron now moves fast forward and spirals around the propagation direction of the laser. This situation is depicted in Fig. 2(b). Note that the amplitude of the electron's transverse motion increases as it advances forward, and that the wiggles on the trajectory diminish by comparison to the off-resonance case. Note also that in producing Fig. 2(b), Eq. (20) has been used to eliminate γ_0 and β_0 from Eqs. (22)–(24) in favor of ω_c and ω_l. This amounts to fixing the initial energy with which the electron is injected into the laser field. For example, this elimination in effect requires that the electron be preaccelerated to an energy of roughly 114 MeV for $B_s = 30$ T and $\lambda = 800$ nm.

The case of exact resonance, $r = 1$, deserves some more scrutiny. To begin with, the expressions for $x(\eta)$, $y(\eta)$, and $z(\eta)$ given in Eqs. (22)–(24) possess exact analytic limits as one lets r go to unity. In this limit, the coordinates are given by the following (much simpler) parametric expressions:

$$x_{lin}(\eta) \to x_{lin}^{res}(\eta) = \frac{qc}{2\omega_c}[\eta \cos\eta - \sin\eta], \tag{25}$$

$$y_{lin}(\eta) \to y_{lin}^{res}(\eta) = \frac{qc}{2\omega_c}[\eta \sin\eta + 2\cos\eta - 2], \tag{26}$$

$$z_{lin}(\eta) \to z_{lin}^{res}(\eta) = \frac{c}{\omega_l}\left\{\left(\frac{\omega_l^2 - \omega_c^2}{2\omega_c^2}\right)\eta + \frac{q^2}{24}\left(\frac{\omega_l}{\omega_c}\right)^2 \eta^3\right\}. \tag{27}$$

Here, too, in arriving at Eqs. (25)–(27), Eq. (20) has been used to eliminate γ_0 and β_0 in favor of ω_c and ω_l. Figure 2(c) shows the trajectory of a single electron in the environment specified by the parameter set employed to produce Fig. 2(b), albeit for $r = 1$ on the basis of Eqs. (25)–(27). Note that Figs. 2(b) and 2(c) are almost identical. This seems to suggest that one in fact does not need to hit exact resonance in order to see the dramatic change in the electron dynamics, which will be shown in Sec. III below to be accompanied by high-electron-energy gains.

C. Circular polarization

As pointed out in Sec. I a linearly polarized wave is equivalent to two circularly polarized components, each of them carrying half of the total intensity. The interaction considered in Sec. II B, which will be shown below to lead to high acceleration in the linearly polarized case, is effectively with the component of the wave corotating with the electron. This, however, has not been explicitly shown above. In other words, we have not decomposed the linearly polarized wave into two components, nor have we thrown away the component counter-rotating with the electron. Thus all quantities pertinent to this problem (the trajectories, that have been discussed above, as well as the other quantities to be dealt with below) are analyzed *exactly* assuming the presence of both components. The circularly polarized case *per se* will

be considered separately, not only for the purpose of completeness, but also because the equations governing the dynamics in this case may not be written down with a little amount of hindsight from the corresponding equations applicable in the linearly polarized case, and vice versa. Furthermore, the circularly polarized wave makes available for interaction with the rotating electron almost twice the amount of radiant energy that the linearly polarized wave of the same amplitude does. As a result, the electron will absorb almost twice as much energy from the circularly polarized wave than from the linearly polarized wave. This will also be demonstrated below in terms of the length, along the forward direction of motion, of the resulting trajectory.

For a plane-wave circularly polarized laser field, we use the value $\delta = 1/\sqrt{2}$ for the ellipticity parameter. Thus the vector potential in this case becomes

$$\mathbf{A}(\eta) = \frac{A_l}{\sqrt{2}}[\hat{\mathbf{i}}\cos\eta + \hat{\mathbf{j}}\sin\eta] - \frac{B_s}{2}(\hat{\mathbf{i}}y - \hat{\mathbf{j}}x). \tag{28}$$

Expressions for $x(\eta)$ and $y(\eta)$ may next be obtained from Eqs. (17) and (18) by inserting the initial conditions. Furthermore, $z(\eta)$ follows along lines similar to those leading to Eq. (24) and described in Ref. [14]. When this has been done, one obtains

$$x_{cir}(\eta) = \frac{qc}{\omega_l\sqrt{2}}\gamma_0(1+\beta_0)\left[\frac{r\sin\eta - \sin(r\eta)}{r(1-r)}\right], \tag{29}$$

$$y_{cir}(\eta) = \frac{qc}{\omega_l\sqrt{2}}\gamma_0(1+\beta_0)\left[\frac{-r\cos\eta + \cos(r\eta) + r - 1}{r(1-r)}\right], \tag{30}$$

$$z_{cir}(\eta) = \frac{c}{\omega_l}\left(\frac{1+\beta_0}{1-\beta_0}\right)\left\{\left[\frac{\beta_0}{1+\beta_0} + \frac{q^2}{2}\frac{1}{(1-r)^2}\right]\eta - \frac{q^2}{2}\frac{\sin[(1-r)\eta]}{(1-r)^3}\right\}. \tag{31}$$

In Fig. 3(a) we show the 3D trajectory parametrized by Eqs. (29)–(31). Note that the electron follows a helical path bearing the same features as that of Fig. 2(a) for the linear polarization case, only its size is larger. This, too, seems to suggest that the electron absorbs more energy from the circularly polarized wave than it does from the linearly polarized one, all other parameters being the same.

The same set of parameters used to produce Fig. 2(a) was used in Fig. 3(a). On the other hand, Fig. 3(b) shows a 3D trajectory in the near-resonance scenario. It corresponds to Fig. 2(b), albeit in the circularly polarized plane-wave laser field.

One may now proceed to the cyclotron resonance limit $r \to 1$ without much difficulty. The following parametric equations for the electron trajectory in the uniform magnetic field and the circularly polarized plane-wave laser field are obtained when the resonance condition is met exactly:

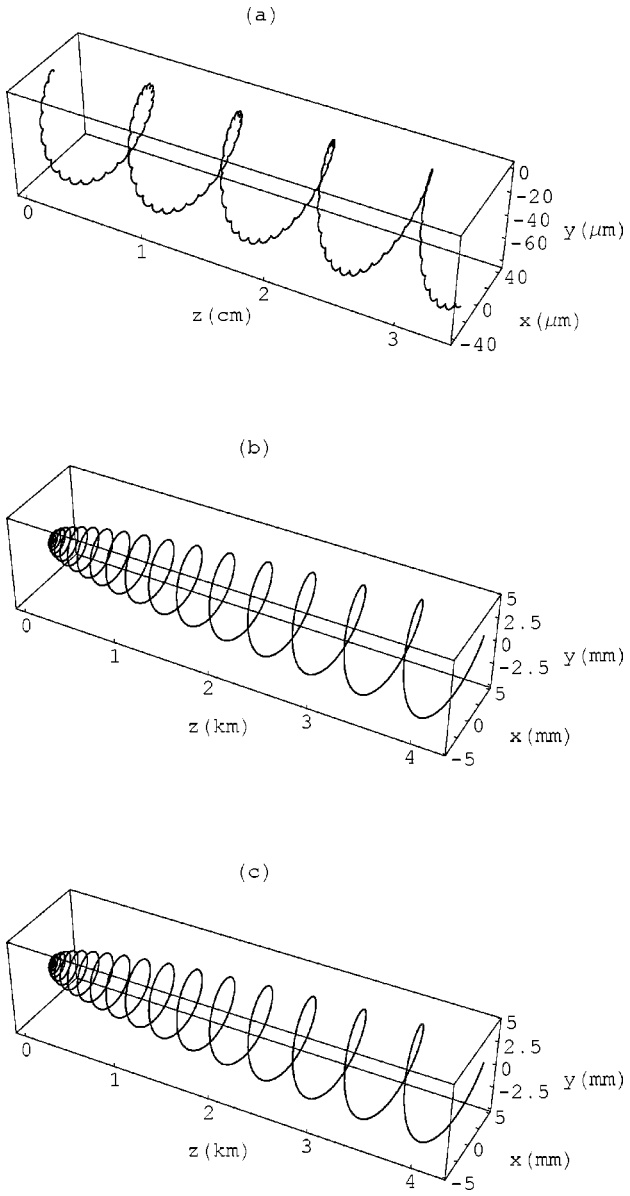

FIG. 3. Same as Fig. 2, but in a plane-wave circularly polarized laser field and a uniform magnetic field.

$$x_{cir}(\eta) \to x_{cir}^{res}(\eta) = \frac{qc}{\omega_c\sqrt{2}}(\eta\cos\eta - \sin\eta), \tag{32}$$

$$y_{cir}(\eta) \to y_{cir}^{res}(\eta) = \frac{qc}{\omega_c\sqrt{2}}(\eta\sin\eta + \cos\eta - 1), \tag{33}$$

$$z_{cir}(\eta) \to z_{cir}^{res}(\eta) = \frac{c}{\omega_l}\left\{\left(\frac{\omega_l^2 - \omega_c^2}{2\omega_c^2}\right)\eta + \frac{q^2}{12}\left(\frac{\omega_l}{\omega_c}\right)^2\eta^3\right\}. \tag{34}$$

Equations (32)–(34) were used to produce Fig. 3(c) for a parameter set the same as that of Fig. 3(b). Note that Figs. 3(b) and 3(c) present nearly identical results, thus lending more support to the thought expressed earlier that exact resonance is perhaps not necessary for reaching a certain high-

energy target; near-resonance may be just as good. The fact that Figs. 2(b) and 2(c), on the one hand, and Figs. 3(b) and 3(c), on the other hand, are almost identical may also be viewed as a numerical check that the limits, evaluated analytically, are correct.

To sum up, we have shown in this section that the highly symmetric wiggly helical trajectories, of an electron in a laser plus uniform magnetic fields, change dramatically when the field parameters conspire with the initial conditions in order to render the electron cyclotron frequency in the uniform magnetic field equal exactly, or even approximately, to the Doppler-shifted frequency of the laser. The correctness of our derivation of the trajectory equations under the condition of exact resonance has also been demonstrated numerically. In Sec. III we show that the dramatic change in the electron trajectories, as a result of the resonance condition being met, is accompanied by tremendous net energy gains by the electron from the radiation field.

III. ELECTRON ENERGY EQUATIONS

A. Cyclotron autoresonance

According to the Lawson-Woodward (LW) theorem (see Ref. [3] for a review), an electron is capable of gaining no net energy as a result of interaction with an electromagnetic (laser, in the present context) field provided the following conditions are met: (1) interaction takes place in vacuum, (2) the electron is highly relativistic $\beta_0 \approx 1$, (3) the ponderomotive effects like the $\boldsymbol{v}\times\boldsymbol{B}$ force are negligible, (4) no static electric or magnetic fields are present, and (5) the interaction region is infinite in extension. Recall that the trajectory equations derived above describe motion of the electron in vacuum, so condition (1) of the LW theorem is satisfied. Condition (2) is already approximately met for an electron injected initially with an energy of a few MeV's. However, for laser-field intensities of the order of 10^{18} W/cm^2 or higher (corresponding to $q \geqslant 1$) the ponderomotive effects are no longer negligible, e.g., the (laser) magnetic force is comparable in strength to its electric counterpart. Thus condition (3) is violated. Moreover, addition of the static magnetic field B_s violates condition (4). Finally, we are interested in accelerating the electron using state-of-the-art short laser pulses; thus, in a practical situation, at most a few laser cycles will be available for interaction with the electron. This violates condition (5) of the LW theorem.

We explain the resonance condition, and the resulting net energy gain when it is met exactly, as follows. For the set of initial conditions adopted in this work, $\beta_{z0}=\beta_0$ and Eq. (10) takes the form

$$\gamma(1-\beta_z)=\gamma_0(1-\beta_0). \tag{35}$$

Multiplying both sides of this equation by mc makes it equivalent to the statement that the quantity $\mathcal{E}/c-p_z$ is a constant of the motion, with $\mathcal{E}$ the total electron energy and p_z the z (forward) component of its momentum. More importantly, Eq. (35) may be written as

$$\frac{(1-\beta_z)}{\sqrt{1-\beta^2}}=\sqrt{\frac{1-\beta_0}{1+\beta_0}}, \tag{36}$$

where $\beta^2=\beta_x^2+\beta_y^2+\beta_z^2$. It will be shown shortly that, in the ALA regime, β_x and β_y are small compared with β_z. Hence $\beta^2 \approx \beta_z^2$. When this result is substituted back into Eq. (36), and after both sides of the resulting equation are multiplied by ω_l, we obtain

$$\tilde{\omega}=\omega_l\sqrt{\frac{1-\beta_z}{1+\beta_z}}\approx\omega_l\sqrt{\frac{1-\beta_0}{1+\beta_0}}=\tilde{\omega}_0, \tag{37}$$

where $\tilde{\omega}$ stands for the Doppler-shifted laser frequency as seen by an observer moving along the z axis at β_z, and $\tilde{\omega}_0$ is the value of $\tilde{\omega}$ at $t=0$. Equation (37) effectively states that the electron ''sees'' a constant Doppler-shifted laser frequency in the forward direction. Recall that the electric component of the circularly polarized laser field rotates around the propagation direction $\mathbf{k}$ at a rate equal to the laser frequency $\omega_l/2\pi$. As viewed by an observer traveling at β_z along $\mathbf{k}$, $\boldsymbol{E}_l$ will be rotating at $\tilde{\omega}/2\pi$. Furthermore, the electron gyrates around the lines of the uniform B_s field, themselves parallel to $\mathbf{k}$, at a rate given by the cyclotron frequency $\omega_c/2\pi$. Consider what happens when conditions are such that $\omega_c=\tilde{\omega}$. In this regime, the instantaneous direction of motion of the electron (i.e., the instantaneous direction of its velocity vector $\boldsymbol{v}$) will maintain the same angle (call it ξ) with the direction of $\boldsymbol{E}_l$. Better yet, if the initial conditions are such that $\omega_c=\tilde{\omega}_0$, then Eq. (37) guarantees that $\omega_c=\tilde{\omega}$, i.e., cyclotron resonance will hold at all times. Consequently, according to Eq. (2), the electron will absorb energy and be accelerated continuously, as long as $\pi/2<\xi<3\pi/2$. For values of ξ outside this range, $d\mathcal{E}/dt$ is negative, i.e, the electron loses energy and decelerates. Obviously, the absorption rate will be a maximum when $\xi=\pi$. This purely intuitive picture may not easily be pushed further. While one may conclude without difficulty that, initially, $\xi_0=\pi/2$, the analysis presented in this paper does not lead to definitive predictions concerning the evolution of ξ with time (or with η). Perhaps it is sufficient to note that immediately after injection into the region of interaction the electron developes a large transverse velocity component (see Figs. 7 and 8) almost opposite in direction to $\boldsymbol{E}_l$. Hence, during that small fraction of the interaction time, the condition $\pi/2<\xi<3\pi/2$ is guaranteed to hold. Subsequently, the transverse velocity components diminish but do not vanish entirely.

The arguments of the previous paragraph were presented for a circularly polarized laser field. They hold equally as well for a linearly polarized field, because the latter may be viewed as the superposition of a left- and right-handed circularly polarized waves, albeit with half the intensity each. Thus it should not be surprising to find out that the electron will gain from a circularly polarized laser field almost twice the amount of energy it would gain from interaction with a linearly polarized one of the same amplitude. This will be demonstrated shortly. We now present the electron energy

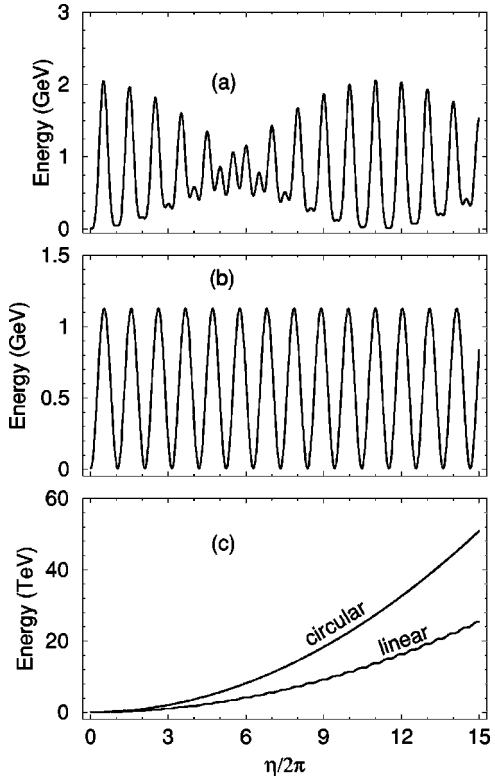

FIG. 4. Electron energy in a plane-wave laser field and a uniform magnetic field vs the number of field cycles. The parameters are wavelength $\lambda = 800$ nm, intensity $I \approx 10^{20}$ W/cm^2 (or $q = 10$), number of field cycles 15, and $B_s = 30$ T. (a) The off-resonance linearly polarized case, with $\gamma_0 = 10$ ($E_0 \approx 4.5$ MeV) and hence $r \approx 0.044612$. (b) The off-resonance circularly polarized case, and the same injection energy as in (a). (c) Exact resonance $r = 1$, and an injection energy of approximately 114.6 MeV.

equations in general, and then show that they take on simpler forms when the cyclotron resonance condition is met.

B. Linear polarization

In Ref. [14], the energy of the electron, scaled by its rest energy mc^2, was given as a function of η by

$$\gamma_{lin}(\eta) = \gamma_0 \left\{ 1 + \frac{1}{2} q^2 (1+\beta_0) \times \left[\frac{(\cos\eta - \cos(r\eta))^2 + (r\sin\eta - \sin(r\eta))^2}{(1-r^2)^2} \right] \right\}. \tag{38}$$

The scaled electron energy is in general an oscillating function of the phase η. Figure 4(a) shows that an electron injected initially with a kinetic energy of about 4.5 MeV is accelerated to a final energy of more than 1.5 GeV after interaction with 15 field cycles. Note also that not all of the energy gained during interaction with the first half-cycle is lost during interaction with the subsequent half-cycle, but that a small part of it is retained. Thus a net energy gain continues to build up until roughly the end of the fifth field cycle. This is followed by a reversal of the process (more loss than gain) during about the next five field cycles, and so on. Based on the discussion, presented above, of the LW theorem it should come as no surprise that the electron emerges from the interaction region with a net gain in energy.

In the situation corresponding to exact resonance, the scaled energy becomes

$$\gamma_{lin}(\eta) \to \gamma_{lin}^{res}(\eta) = \frac{\omega_l^2 + \omega_c^2}{2\omega_l\omega_c} \left\{ 1 + \frac{q^2}{4} \left[\frac{\omega_l^2}{\omega_l^2 + \omega_c^2} \right] \eta^2 \right\} + \frac{q^2}{8} \left(\frac{\omega_l}{\omega_c} \right) \{ \sin^2\eta - \eta \sin 2\eta \}. \tag{39}$$

This may be obtained by letting $r \to 1$ in Eq. (38), and after β_0 and γ_0 have been eliminated in favor of the laser and cyclotron frequencies. The term proportional to η^2 in this expression is responsible for a monotonic growth in γ, the trigonometric terms merely add extra fine structure.

C. Circular polarization

The case of a circularly polarized plane-wave leads to even simpler expressions for γ. Under fairly general conditions (rendering r arbitrary), in this case we have [14]

$$\gamma_{cir}(\eta) = \gamma_0 \left\{ 1 + q^2 (1+\beta_0) \left[\frac{\sin[(1-r)\eta/2]}{1-r} \right]^2 \right\}. \tag{40}$$

In Fig. 4(b) we show the electron energy versus the number of field cycles based on Eq. (40), and employing the set of parameters of Fig. 4(a). Note that the extrema in this figure are shifted continuously toward the left; thus the electron emerges at the end of interaction with the fifteenth field cycle with an energy gain of roughly 0.8 GeV. In order to understand the distinction between Figs. 4(a) and 4(b), recall that the linearly polarized plane wave may be decomposed into two circularly polarized waves with two counter-rotating electric field vectors. Thus the right-hand side of Eq. (2) for this case consists of two sinusoidal terms, one for each of these vectors. When this equation is ultimately integrated, the algebraic sum of the two equal-amplitude sinusoidal terms gives rise to the beat structure exhibited in Fig. 4(a). On the other hand, in the circularly polarized case, the right-hand side of Eq. (2) contains a single sinusoidal term; hence the sinusoidal behavior of Fig. 4(b).

On resonance, $r \to 1$, and the scaled energy becomes

$$\gamma_{cir}(\eta) \to \gamma_{cir}^{res}(\eta) = \frac{\omega_l^2 + \omega_c^2}{2\omega_l\omega_c} \left\{ 1 + \frac{q^2}{2} \left[\frac{\omega_l^2}{\omega_l^2 + \omega_c^2} \right] \eta^2 \right\}. \tag{41}$$

Thus the scaled energy in this case increases monotonically with η, all oscillatory behavior is absent.

In Fig. 4(c) we show the variation of the electron energy with the number of field cycles for both cases of polarization when the resonance condition is met exactly, i.e., on the basis of Eqs. (39) and (41). Note that the net energy gain

after interaction with the full laser pulse depends on the total number of field cycles in that pulse; hence one obtains more energy by simply increasing the number of field cycles in the pulse employed. This, however, is not practical, as will be illustrated shortly, in that it leads to a prohibitively long interaction region. The gain in energy is diffusive in both space and time. In this context, Fig. 4 is only meant to illustrate the main ideas, and may not necessarily correspond to practically realizable situations.

D. Discussion

We have seen in Sec. III C that a MeV electron may reach GeV energies as a result of interaction with part or all of a plane-wave pulse (with a suitably designed turn-on and turn-off). This has been shown to be possible when present-day laser intensities are employed, and in the added presence of a uniform magnetic field whose strength is also available for today's laboratory experiments. It was also demonstrated that TeV energies may in principle be reached if the electron is launched initially into cyclotron resonance with the laser field. We now show that absorption of energy from the radiation field takes place over a long distance, and that in order to reach TeV energies the need arises for laser pulses containing a small number of field cycles.

Figure 5, for example, shows the electron energy versus the forward distance along the z axis over which the electron advances during interaction with a pulse containing only three half-cycles. For all graphs shown, $B_s = 30$ T, and q is increased from a value of unity ($I \approx 10^{18}$ W/cm^2) to 100 ($I \approx 10^{22}$ W/cm^2). The dependence upon q (and hence the intensity I) is predictable: Eqs. (39) and (41) show that the energy scales as $q^2 \approx I$. So, in going from Figs. 5(a) to 5(b), I increases by two orders of magnitude, and so does the maximum (exit) electron energy. The same behavior is encountered in going from Figs. 5(b) to 5(c).

The lines in Fig. 5 corresponding to the linear polarization case very clearly show the energy gain during interaction with each half-cycle. Note that the electron is accelerated during encounter with each half-cycle; no net deceleration is exhibited. Furthermore, as it absorbs energy, the electron picks up speed and its forward excursions, during interaction with the successive half-field cycles, become successively longer. The total forward excursion, measured between the coordinate origin and the point on the z axis at which the electron is left behind the trailing edge of the pulse, increases with increasing field intensity.

Note also that the exit electron energy in the circular polarization case is almost double that of the linear polarization in each graph. But there is a price for this; namely, the forward excursion in the circular polarization case is almost twice that in the linear polarization case. Thus, we conclude that the combination of high-intensity and circular polarization leads, in general, to high-energy electron acceleration. Unfortunately, this quickly makes the net forward excursion, and hence the length of the accelerator, too impractical.

The goal is to reach TeV energies, utilizing the ultra-high-intensity laser pulses available today, without making the accelerator too long. In trying to optimize the conditions under which this goal may be achieved, we investigate the effect of the magnetic field on the process of acceleration. While it does not change the electron energy, the value of B_s plays a sensitive role in determining the initial injection energy needed to meet the resonance condition. This initial injection energy then uniquely determines the energy with which the electron emerges from the interaction region. To elucidate this point, consider Fig. 6. In this figure, the energy is shown versus the forward distance of travel during interaction with linearly and circularly polarized pulses containing three half-cycles and having an intensity $I \approx 10^{22}$ W/cm^2 (q=100). The plots in Figs. 6(a)–6(c) differ only in the value of B_s, and hence in the injection energy $\mathcal{E}_0 = \gamma_0 mc^2$, due to the resonance condition. For example, a 68.8-MeV electron may be accelerated to 30 TeV by the circularly polarized pulse and in the presence of a uniform magnetic field of strength $B_s = 50$ T, over a distance of roughly 6.4 km. How-

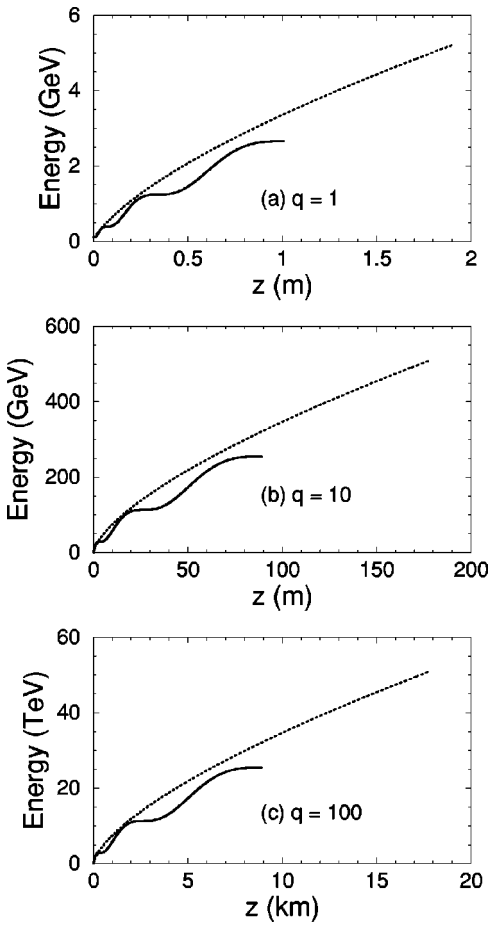

FIG. 5. Electron energy in a plane-wave laser field and a uniform magnetic field in the ALA regime vs the forward distance along $+z$ over which interaction takes place. The continuous lines are linear polarization cases, and the dotted lines represent circular polarization. The parameters are wavelength $\lambda = 800$ nm, number of field cycles 1.5, and $B_s = 30$ T. (a) Intensity $I \approx 10^{18}$ W/cm^2 (or $q = 1$). (b) $I \approx 10^{20}$ W/cm^2 (or $q = 10$). (c) $I \approx 10^{22}$ W/cm^2 (or $q = 100$). Effectively, these are plots of $\mathcal{E}(\eta)$ vs $z(\eta)$ parametrized by η. In other words, data for these plots have been produced by evaluating the functions $\mathcal{E}(\eta)$ and $z(\eta)$ over η values ranging between 0 and 3π.

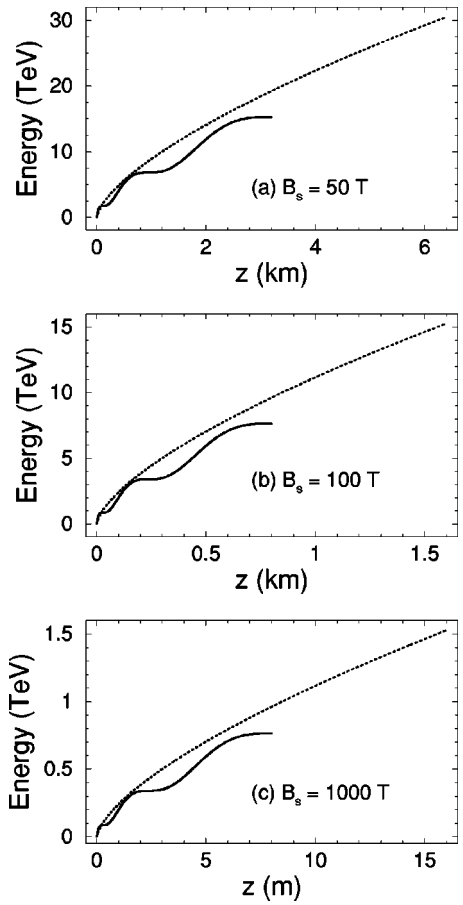

FIG. 6. Same as Fig. 5, but for $q=100$ and different values of B_s.

ever, a maximum of about 15 TeV may be reached over almost 1.7 km for $B_s=100$ T, but only if the electron is preaccelerated to $\mathcal{E}_0\approx 34.4$ MeV. Likewise, Fig. 6(c) shows that in a $B_s=1000$ T magnetic field (perhaps a leap into the future) a 3.46-MeV electron may reach 1.5 TeV over a distance of only 17 m.

The results presented above have emerged from a single-particle analysis. A realistic situation will probably involve an assembly of electrons, like in a plasma or an electron beam, with a spread in initial velocities. We close this subsection by making an estimate of the effect on the final electron energy due to the spread in initial electron speeds. Let $\Delta\beta_0$ be the forward speed uncertainty, due to whatever sources, and let $mc^2\Delta\gamma_0$ be the corresponding spread in initial injection energy. It is then straightforward to show that

$$\Delta\beta_0=\frac{\Delta\gamma_0}{\beta_0\gamma_0^3}. \tag{42}$$

To obtain an idea about the effect of the initial-energy spread on the final energy of electrons accelerated by the ALA scheme employing a circularly polarized laser wave, we turn to Eq. (40). Writing $\Delta\gamma_{cir}=(\partial\gamma_{cir}/\partial\beta_0)\Delta\beta_0$, then simple differentiation, followed by substitution of the resonance condition in the result, yields

$$\Delta\gamma_{cir}=\Delta\gamma_0\left\{1+\frac{q^2\eta^2}{4}\left(\frac{1+\overline{\beta}_0}{\overline{\beta}_0}\right)\right\}, \tag{43}$$

where $\overline{\beta}_0$ stands for an average value for the initial forward speed that is necessary to meet the autoresonance condition. Furthermore, Eq. (42) has been used in an intermediate step. This then leads to the following expression for the spread in the electron final energy:

$$\frac{\Delta\mathcal{E}_{cir}}{\mathcal{E}_{cir}}=\frac{\Delta\gamma_0}{\gamma_{cir}}\left\{1+\frac{q^2\eta^2}{4}\left(\frac{1+\overline{\beta}_0}{\overline{\beta}_0}\right)\right\}. \tag{44}$$

The corresponding expression applicable in the linearly polarized case follows from Eq. (38) along similar lines. We give it here for completeness:

$$\frac{\Delta\mathcal{E}_{lin}}{\mathcal{E}_{lin}}=\frac{\Delta\gamma_0}{\gamma_{lin}}\left\{1+\frac{q^2\eta^2}{8}\left(\frac{1+\overline{\beta}_0}{\overline{\beta}_0}\right)\sin^2\eta\right\}. \tag{45}$$

As an example, consider the situation depicted in Fig. 6(a). There, $\mathcal{E}_{cir}=\gamma_{cir}mc^2\approx 30$ TeV, $q=100$, $\eta=3\pi$, and $\overline{\beta}_0\approx 0.999972$. Assume a linac electron beam of initial energy spread $mc^2\Delta\gamma_0\approx 2$ MeV. When these numbers are substituted into Eq. (44), one obtains $\Delta\mathcal{E}_{cir}/\mathcal{E}_{cir}\approx 0.03$. Similarly, with $\mathcal{E}_{lin}=\gamma_{lin}mc^2\approx 15$ TeV, Eq. (45) gives $\Delta\mathcal{E}_{lin}/\mathcal{E}_{lin}\approx 1.3\times 10^{-7}$. Thus one may conclude that the initial spread in electron energies has little effect on the ultimate energy of the accelerated electron in the ALA scheme.

IV. RADIATION LOSSES

A. Preliminaries

Our analytic expressions for the electron dynamics have all resulted from the solution of Eqs. (5). In writing down those equations, terms due to radiation reaction have been neglected. It was recently demonstrated [34] that the effect, on the *free*-electron trajectory and other aspects of its motion, of including a radiation reaction term is quite small, even for laser field intensities as high as 10^{22} W/cm^2. This inclusion leads to effects that may be significant near the turning points of the electron motion in the presence of a nuclear center. Another situation in which radiation reaction may be important arises in a trap [35], where the electron cyclotron motion is accompanied by hysteresis due, for example, to interaction with the radiation that in turn results from such processes as collisions with other particles in the trap.

The maximum energy attainable by the electron in an accelerator may be limited by radiation losses that accompany the acceleration process. We investigate the issue of radiation loss in the ALA scheme by employing the relativistic generalization of the Larmor formula [32] for the total instantaneous power emitted by the electron, namely,

$$P(t)=\frac{2}{3}\frac{e^2}{c}\gamma^6\left\{\left[\frac{d\boldsymbol{\beta}}{dt}\right]^2-\left[\boldsymbol{\beta}\times\frac{d\boldsymbol{\beta}}{dt}\right]^2\right\}, \tag{46}$$

where $d\boldsymbol{\beta}/dt$ is the instantaneous acceleration of the electron scaled by the speed of light. We turn $P(t)$ into a function of the phase η using the chain rule of differentiation $d\boldsymbol{\beta}/dt = (d\boldsymbol{\beta}/d\eta)(d\eta/dt)$, and Eq. (19), together with a well-known vector identity. When the resonance condition is used to eliminate the dependence upon the initial velocity, the result is

$$P(\eta) = \frac{2}{3}\frac{(e\omega_c\gamma)^2}{c}\left\{\left[\frac{d\boldsymbol{\beta}}{d\eta}\right]^2 + \gamma^2\left[\boldsymbol{\beta}\cdot\frac{d\boldsymbol{\beta}}{d\eta}\right]^2\right\}. \tag{47}$$

As a qualitative measure of the energy loss, we adopt the quantity $\Gamma(\eta)$ defined as the ratio of the power radiated to the energy gained during interaction with one cycle of the laser field. In other words,

$$\Gamma(\eta) = \frac{2\pi}{\omega_l}\frac{P}{\mathcal{E}} = \frac{4\pi}{3\omega_l c}\frac{(e\omega_c\gamma)^2}{\gamma mc^2}\left\{\left[\frac{d\boldsymbol{\beta}}{d\eta}\right]^2 + \gamma^2\left[\boldsymbol{\beta}\cdot\frac{d\boldsymbol{\beta}}{d\eta}\right]^2\right\}. \tag{48}$$

In the next two subsections we derive expressions for the electron velocity components. These expressions will be later used to compute $\Gamma(\eta)$ on the basis of Eq. (48).

B. Linear polarization

Inserting $\delta = 1$ and using the initial conditions in Eqs. (10), (13), and (14) yields the following:

$$(\gamma\beta_x)_{lin}(\eta) = q(\cos\eta - 1) - \frac{\omega_c}{c}y_{lin}(\eta), \tag{49}$$

$$(\gamma\beta_y)_{lin}(\eta) = \frac{\omega_c}{c}x_{lin}(\eta), \tag{50}$$

$$(\gamma\beta_z)_{lin}(\eta) = \gamma_{lin}(\eta) - \gamma_0(1-\beta_0). \tag{51}$$

When the expressions valid under the autoresonance condition for $x(\eta)$,$y(\eta)$, and $\gamma(\eta)$, respectively—namely Eqs. (25), (26), and (39)—are used in Eqs. (49)–(51), the results are

$$\beta^{res}_{x,lin}(\eta) = -\frac{q}{2}\left[\frac{\eta\sin\eta}{\gamma^{res}_{lin}(\eta)}\right], \tag{52}$$

$$\beta^{res}_{y,lin}(\eta) = \frac{q}{2}\left[\frac{\eta\cos\eta - \sin\eta}{\gamma^{res}_{lin}(\eta)}\right], \tag{53}$$

$$\beta^{res}_{z,lin}(\eta) = 1 - \left[\frac{\omega_c/\omega_l}{\gamma^{res}_{lin}(\eta)}\right]. \tag{54}$$

Figure 7 presents the components of $\boldsymbol{\beta}^{res}_{lin}$ for q=100, $\lambda = 800$ nm, and $B_s = 100$ T [the set of parameters employed to produce the line in Fig. 6(b), corresponding to linear polarization]. The plots are given for interaction with five field cycles. Note that the transverse components diminish by comparison to the longitudinal one as interaction with the field progresses. This justifies the approximation leading to

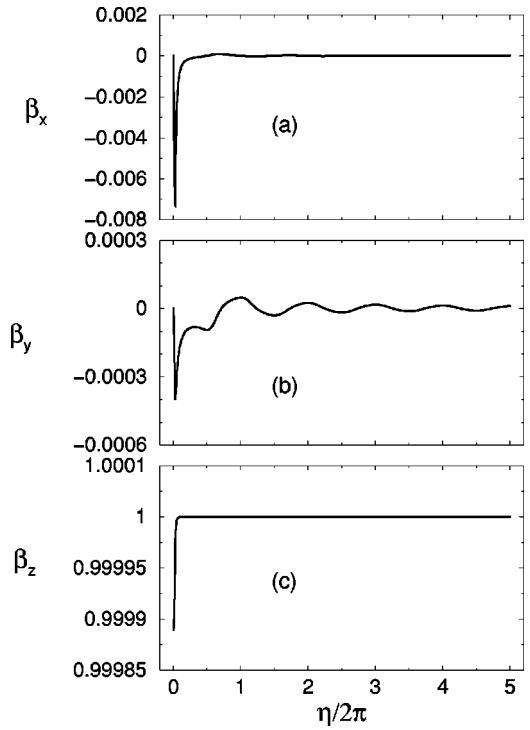

FIG. 7. Components of the electron velocity vector scaled by the speed of light in vacuum vs the number of field cycles. Shown here is the case of interaction with five field cycles of a linearly polarized plane-wave laser field. The other parameters are wavelength $\lambda = 800$ nm, $B_s = 100$ T, and intensity $I \approx 10^{22}$ W/cm^2 (or $q = 100$).

Eq. (37), which we used only to illustrate the resonance condition and to enhance the intuitive picture built upon it. At $t = 0$ the laser electric force $\boldsymbol{F}_e$ on the electron points in the $-x$ direction, while the magnetic force $\boldsymbol{F}_m$ points along $+x$. Hence, since $F_e > F_m$ at that point, the electron velocity vector will quickly acquire a transverse component. At later points, however, F_m becomes comparable in magnitude to F_e and may be decomposed into transverse and longitudinal components. The longitudinal component works to accelerate the electron in the forward direction $(+z)$.

C. Circular polarization

Similarly, when the value $\delta = 1/\sqrt{2}$ and the initial conditions are inserted in Eqs. (10), (13), and (14) the following set of equations is obtained:

$$(\gamma\beta_x)_{cir}(\eta) = \frac{q}{\sqrt{2}}(\cos\eta - 1) - \frac{\omega_c}{c}y_{cir}(\eta), \tag{55}$$

$$(\gamma\beta_y)_{cir}(\eta) = \frac{q}{\sqrt{2}}\sin\eta + \frac{\omega_c}{c}x_{cir}(\eta), \tag{56}$$

$$(\gamma\beta_z)_{cir}(\eta) = \gamma_{cir}(\eta) - \gamma_0(1-\beta_0). \tag{57}$$

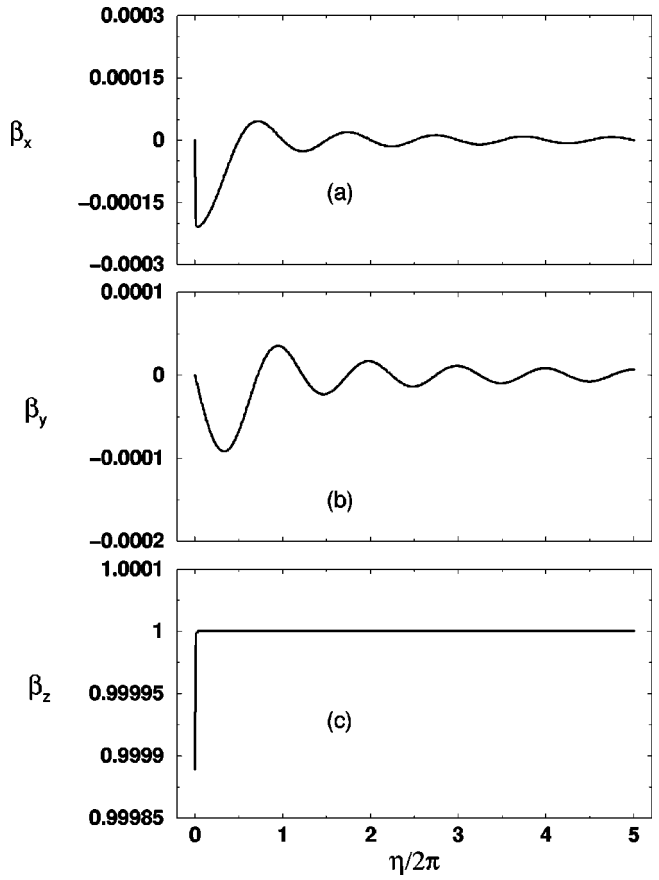

FIG. 8. Same as Fig. 7, but in a circularly polarized plane-wave laser field.

When the expressions for $x(\eta)$,$y(\eta)$, and $\gamma(\eta)$, namely, Eqs. (32), (33), and (41), which are valid under the autoresonance condition, are used in Eqs. (55)–(57), the results are

$$\beta_{x,cir}^{res}(\eta) = -\frac{q}{\sqrt{2}}\left[\frac{\eta \sin \eta}{\gamma_{cir}^{res}(\eta)}\right], \tag{58}$$

$$\beta_{y,cir}^{res}(\eta) = \frac{q}{\sqrt{2}}\left[\frac{\eta \cos \eta - \sin \eta}{\gamma_{cir}^{res}(\eta)}\right], \tag{59}$$

$$\beta_{z,cir}^{res}(\eta) = 1 - \left[\frac{\omega_c/\omega_l}{\gamma_{cir}^{res}(\eta)}\right]. \tag{60}$$

Equations (58)–(60) are presented graphically in Fig. 8 for the same set of parameters that Fig. 7. Here, too, we note that the transverse components diminish after interaction with the first few field half-cycles, and $\beta_{z,cir}^{res}(\eta)$ approaches unity.

D. Some estimates

With Eqs. (52)–(54) and (58)–(60) at hand, we are now ready to make a reasonable estimate of the radiation losses. We will employ Eq. (48) for this task, as promised earlier. The cases we consider are those of boosting a 34.4-MeV electron to TeV final energies using laser pulses containing 1.5 field cycles (intensity $\approx 10^{22}$ W/cm^2 and wavelength $\lambda = 800$ nm) and in the added presence of a uniform magnetic field of strength 100 T. This is the case we presented in Fig. 6(b). The final energy is 15 TeV in the circular polarization case, and about half that much in the linearly polarized one. But in both cases, the energy gradient is almost the same (roughly 10 GeV/m).

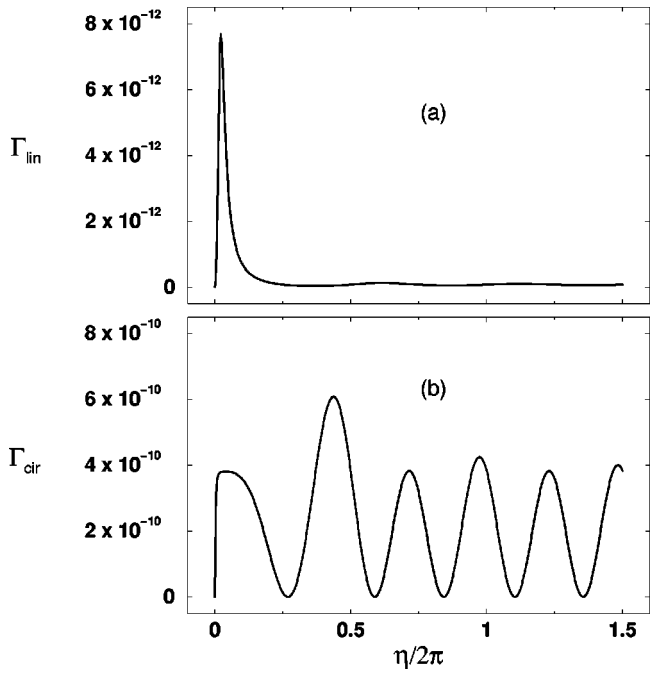

FIG. 9. Ratio of the radiation loss to energy gain per interaction with a single field cycle, vs the number of field cycles. Shown here is the case of Fig. 6(b). (a) The linear polarization case. (b) The circular polarization case.

In Fig. 9 we show the quantity Γ, defined in Eq. (48) above, versus the number of laser-field cycles for both cases of laser-field polarization. It is obvious from both parts that the highest loss ratio characterizes interaction with only a fraction of the first field cycle, and is itself very small. Subsequently the loss ratio diminishes, in the linear polarization case, and oscillates, albeit with a vanishingly small amplitude, in the case of acceleration in the circularly polarized pulse. The final conclusion is that the radiation losses in the ALA scheme, based on our equations, are negligibly small when compared with the electron energy gain at any space-time point during the acceleration process. We also take a hint from the oscillatory character of Fig. 9(b) that the emitted radiation may contain harmonics of the laser-field frequency. This is the subject of Sec. V.

V. EMISSION SPECTRA

The estimates made at the end of Sec. IV showed that a small fraction of the radiation absorbed by the electron will be re-emitted. The weak radiation scattered in this way has an interesting frequency distribution. In this section we study the spectra of the emitted radiation on the basis of the equation [32]

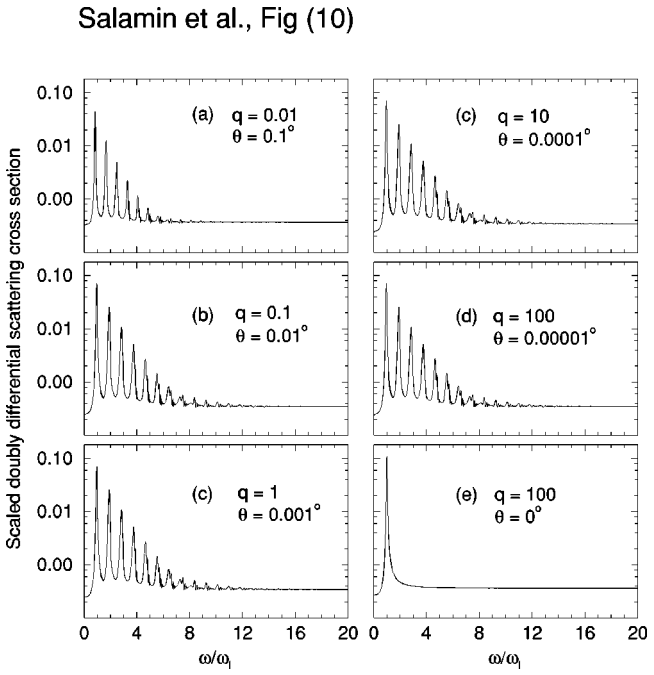

FIG. 10. Spectra for observation at a small angle θ with the forward direction ($+z$ axis) calculated for interaction with 20 field cycles of a plane-wave circularly polarized pulse. Wavelength $\lambda = 800$ nm, and the intensity begins in (a) at $I \approx 10^{14}$ W/cm^2, and increases by two orders of magnitude in the succeeding graphs to $I \approx 10^{22}$ W/cm^2 in (f). $B_s = 30$ T.

$$\frac{d^2E(\omega,\Omega)}{d\Omega d\omega} = \frac{e^2}{4\pi^2 c}\left| \int_0^T \frac{\hat{\mathbf{n}}\times[\hat{\mathbf{n}}-\boldsymbol{\beta}(t)]\times\dot{\boldsymbol{\beta}}(t)}{[1-\hat{\mathbf{n}}\cdot\boldsymbol{\beta}(t)]^2} \times \exp\left\{ i\omega\left[t - \frac{\hat{\mathbf{n}}\cdot\mathbf{r}(t)}{c}\right]\right\} dt \right|^2, \tag{61}$$

where E is used here to denote the radiated energy, $\hat{\mathbf{n}}$ is a unit vector in the direction of propagation of the emitted radiation (direction of observation), $\dot{\boldsymbol{\beta}}$ is the particle acceleration divided by the speed of light, and T is the time interval over which interaction between the electron and the laser field takes place. In what follows, we will report the spectra in terms of the scaled doubly differential scattering cross section, given by

$$\frac{1}{r_0^2}\frac{d^2\sigma(\omega,\Omega)}{d\Omega d\omega} = \frac{1}{T}\frac{8\pi c}{(eq\omega_l)^2}\frac{d^2E(\omega,\Omega)}{d\Omega d\omega}. \tag{62}$$

This quantity was obtained by dividing the radiant energy, emitted into a unit solid angle $d\Omega$ about $\hat{\mathbf{n}}$ per unit frequency interval $d\omega$ per unit time, by the incident energy flux, $(eq\omega_l)^2/8\pi c r_0^2$, r_0 being the classical electron radius. An integration by parts may next be performed on Eq. (61) which, when followed by a change of variable from t to η, results in

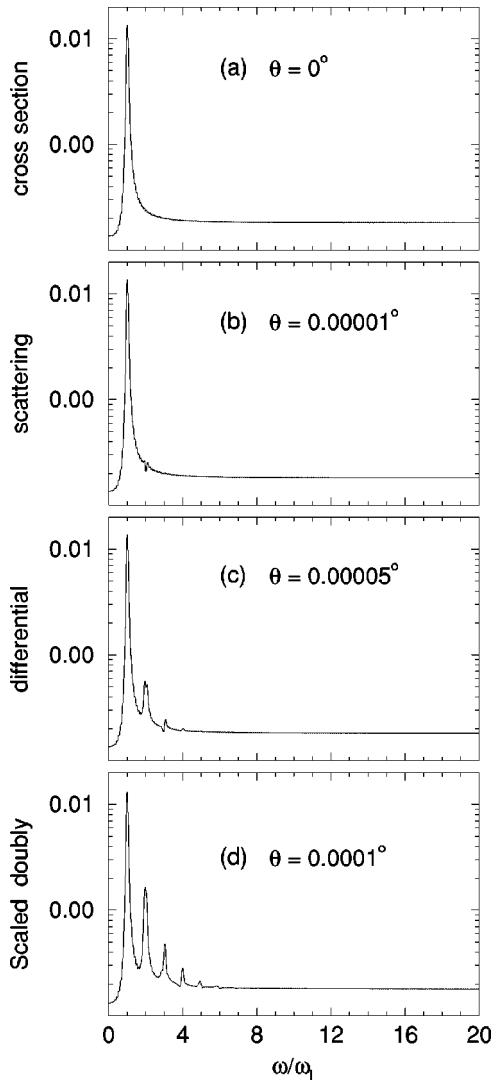

FIG. 11. Spectra for observation at a small angle θ with the forward direction ($+z$ axis) calculated for interaction with ten field cycles of a plane-wave circularly polarized pulse of intensity $I \approx 10^{20}$ W/cm^2 (or $q = 10$). The remaining parameters are wavelength $\lambda = 800$ nm and $B_s = 30$ T.

$$\frac{1}{r_0^2}\frac{d^2\sigma(\omega,\Omega)}{d\Omega d\omega} = \frac{\omega_l}{N(q\pi\omega_l)^2}\left| \boldsymbol{F}(\omega) - i\left(\frac{\omega}{\omega_l}\right)\boldsymbol{G}(\omega)\right|^2, \tag{63}$$

where

$$\boldsymbol{F}(\omega) = \left[\frac{\hat{\mathbf{n}}\times\hat{\mathbf{n}}\times\boldsymbol{\beta}(\eta)}{1-\hat{\mathbf{n}}\cdot\boldsymbol{\beta}(\eta)}\right]\exp\left\{ i\frac{\omega}{\omega_l}\left[\eta + \frac{\omega_l}{c} \times[z(\eta)-\hat{\mathbf{n}}\cdot\mathbf{r}(\eta)]\right]\right\}\Bigg|_0^{2\pi N}, \tag{64}$$

$$\boldsymbol{G}(\omega) = \frac{\omega_l}{c}\int_0^{2\pi N}\left[\hat{\mathbf{n}}\times\hat{\mathbf{n}}\times\frac{d\mathbf{r}}{d\eta}\right]\exp\left\{ i\frac{\omega}{\omega_l}\left[\eta + \frac{\omega_l}{c} \times[z(\eta)-\hat{\mathbf{n}}\cdot\mathbf{r}(\eta)]\right]\right\} d\eta. \tag{65}$$

In spherical polar coordinates, $\hat{\mathbf{n}}=(\sin\theta\cos\phi,\sin\theta\sin\phi,\cos\theta)$. Analytical calculation of the spectrum corresponding to emission along a general direction on the basis of Eqs. (63)–(65) is not straightforward [31], even in the autoresonance scenario, save perhaps for very specialized situations. We will therefore evaluate the remaining integral numerically instead.

A. Forward spectrum

This is a trivial case that has been handled analytically in the off-resonance situation [28]. It has been shown that the forward spectrum consists of two peaks, one at the pump frequency ω_l and the other at $r\omega_l$. When conditions for the ALA are met, these two peaks coalesce to give a slightly enhanced peak at the fundamental. Examples are shown in Figs. 10(f) and 11(a).

B. Emission spectrum at a small angle to the forward direction

So far, we have been using the term forward to refer to the $+z$ axis, this being the initial direction of motion of the electron upon injection. During interaction with the field configuration we have been interested in thus far, the electron follows a semihelical trajectory and the instantaneous direction of its motion (taken along the direction of its instantaneous velocity vector) actually makes a small angle with the direction of $+z$ (see Figs. 2 and 3). It is well known that a relativistic electron undergoing acceleration emits radiation mostly in a small cone around its instantaneous direction of motion. We are interested here in the frequency distribution of the radiation emitted by the electron with whose dynamics we have been concerned thus far.

In Fig. 10 we show, for example, the spectra one would most likely observe using a detector facing the origin of coordinates and tilted at a small angle θ with $+z$. Note that, in addition to emission at the fundamental frequency, several more harmonics are shown to be emitted. Two more features are quite evident in the spectra reported in Fig. 10. One feature concerns the direction of emission with increasing field intensity, which agrees with well established facts: with increasing laser-field intensity the electron becomes more and more relativistic, and emits in a cone of smaller and smaller apex angle. Hence we need to look for the emitted radiation at smaller and smaller angles with increasing field intensity. The other feature is a redshift suffered by all the harmonics, because the radiation *seen* by the relativistic electron is actually Doppler shifted.

In order to better elucidate these and other features of the emitted radiation, we have calculated spectra corresponding to a fixed laser-field intensity, but a varying angle of observation. In Fig. 11, we present the spectra one would observe by scattering a plane-wave circularly polarized laser field of intensity $I\approx 10^{20}$ W/cm^2 ($q=10$) from a free electron, in the added presence of a 30-T magnetic field and in the autoresonance scenario. As the angle of observation is increased from zero, where only the line at the fundamental is present, the first harmonic shows up clearly at $\theta=0.00001°$. The second and third harmonics show up clearly at $\theta=0.00005°$, and so on. It seems that other higher harmonics may be seen; one only needs to know at what angle to look for them.

VI. SUMMARY

Exact equations for the electron dynamics in the autoresonance laser accelerator scheme have been developed. It has been shown that MeV electron may be boosted to energies of up to several TeV by a plane-wave ultra-high-intensity laser field, provided it is injected parallel to the lines of a uniform axial magnetic field of strength currently available to laboratory experiments. During the acceleration process the electron emits only a small fraction of the energy gained. It has been shown that the radiation, emitted at a small angle relative to the initial direction of injection of the electron, contains several harmonics of the laser-field frequency, including even-order ones. The presence of the even-order harmonics was attributed earlier [33] to the added axial magnetic field.

This work presented a set of simple equations for the electron dynamics, and related issues, which hopefully help to better understand the mechanism of autoresonance acceleration. They may also serve as a basis for the more realistic description of the mechanism in terms of wave packets.

ACKNOWLEDGMENTS

Y.I.S. gratefully acknowledges support from the DAAD Gastdozentenprgramm at the University of Freiburg. C.H.K. was funded by the German Science Foundation (Nachwuchsgruppe within SFB 276), and F.H.M.F. was partially supported by DFG-SPP: ''Relativistische Effekte.''

[1] W.D. Kimura *et al.*, Phys. Rev. Lett. **74**, 546 (1995).
[2] A. van Steenbergen *et al.*, Phys. Rev. Lett. **77**, 2690 (1996).
[3] E. Esarey, P. Sprangle, and J. Krall, Phys. Rev. E **52**, 5443 (1995).
[4] E. Esarey *et al.*, IEEE Trans. Plasma Sci. **24**, 252 (1996).
[5] K. Nakajima *et al.*, Phys. Rev. Lett. **74**, 4428 (1995).
[6] E. Esarey, B. Hafizi, R. Hubbard, and A. Ting, Phys. Rev. Lett. **80**, 5552 (1998).
[7] A. Ting *et al.*, Phys. Plasmas **4**, 1889 (1997).
[8] C.I. Moore *et al.*, Phys. Rev. Lett. **79**, 3909 (1997).
[9] T. Häuser, W. Scheid, and H. Hora, Phys. Lett. A **186**, 189 (1994).
[10] Y.K. Ho *et al.*, Phys. Lett. A **220**, 189 (1996).
[11] J.X. Wang *et al.*, Phys. Rev. E **58**, 6575 (1998).
[12] D. Gordon *et al.*, Phys. Rev. Lett. **80**, 2133 (1998).
[13] W.E. Baylis and Y. Yao, Phys. Rev. A **60**, 785 (1999).
[14] Y.I. Salamin and F.H.M. Faisal, Phys. Rev. A **58**, 3221 (1998).
[15] Y.I. Salamin and C.H. Keitel, Appl Phys. Lett. **77**, 1082

(2000); Y.A. Salamin and F.H.M. Faisal, Phys. Rev. A **61**, 043801 (2000); Y. Salamin, C.H. Keitel, and F.H.M. Faisal (unpublished).
[16] C.R. Menyuk, A.T. Drobot, K. Papadopoulos, and H. Karimabadi, Phys. Rev. Lett. **58**, 2071 (1987).
[17] C.E. Clayton *et al.*, Phys. Rev. Lett. **70**, 37 (1993).
[18] A.A. Chernikov, G. Schmidt, and A.I. Neishtadt, Phys. Rev. Lett. **68**, 1507 (1992).
[19] M.S. Hussein and M.P. Pato, Phys. Rev. Lett. **68**, 1136 (1992).
[20] M.S. Hussein, M.P. Pato, and A.K. Kerman, Phys. Rev. A **46**, 3562 (1992).
[21] A. Loeb and L. Friedland, Phys. Rev. A **33**, 1828 (1986).
[22] A. Loeb and S. Eliezer, Phys. Rev. Lett. **56**, 2252 (1986).
[23] A. Loeb, L. Friedland, and S. Eliezer, Phys. Rev. A **35**, 1692 (1987).
[24] D.M. Perry *et al.*, Opt. Lett. **24**, 160 (1999).
[25] M. Schnürer *et al.*, Phys. Rev. Lett. **80**, 3236 (1998).
[26] A.A. Kolomenskii and A.N. Lebedev, Zh. Éksp. Teor. Fiz. **44**, 261 (1963) [Sov. Phys. JETP **17**, 179 (1963)].
[27] C.S. Roberts and S.J. Buchsbaum, Phys. Rev. **135**, A381 (1964).
[28] F.H.M. Faisal and Y.I. Salamin, Phys. Rev. A **60**, 2505 (1999).
[29] F.V. Hartemann *et al.*, Phys. Rev. E **58**, 5001 (1998).
[30] Some relevant papers are Y.L. Shao *et al.*, Phys. Rev. Lett. **77**, 3343 (1996); T. Ditmire *et al.*, *ibid.* **78**, 2732 (1997); Nature (London) **386**, 54 (1997); C.H. Keitel, J. Phys. B **29**, L873 (1996); C. Szymanowski *et al.*, Phys. Rev. A **56**, 3846 (1997); C.H. Keitel and P.L. Knight, *ibid.* **51**, 1420 (1995); R.E. Wagnr, Q. Su, and R. Grobe, *ibid.* **60**, 3233 (1999).
[31] Y.I. Salamin, Phys. Rev. A **60**, 3276 (1999).
[32] C.H. Keitel, C. Szymanowski, P.L. Knight, and A. Maquet, J. Phys. B **31**, L75 (1998).
[33] See A.E. Kaplan and Y.J. Ding, IEEE J. Quant. Opt. **24**, 1470 (1988), and references therein.
[34] J. D. Jackson, *Classical Electrodynamics*, 2nd ed. (Wiley, New York, 1975).
[35] J.-P. Connerade and C.H. Keitel, Phys. Rev. A **53**, 2748 (1996).